

Light-Driven Bound State of Interacting Impurities in a Dirac-Like Bath

Vinayak M. Kulkarni

Theoretical Sciences Unit, Jawaharlal Nehru Centre for Advanced Scientific Research Jakkur, Bangalore - 560064, India

(Dated: May 26, 2025)

Recent investigations have revealed the presence of exceptional points in the low-energy effective spin-interacting impurity model, previously explored via non-Hermitian renormalization group (RG) techniques. These studies uncovered novel RG fixed points and linked them to distinct transport signatures. In this work, we revisit the model from a real-time field-theoretic perspective, studying both non-interacting and strongly correlated ($U = \infty$) limits using the exact equation of motion and a Large- N Keldysh variational mean-field approach. Remarkably, we find that the steady-state solutions of the Keldysh action exhibit the same fixed point structure as the RG flows, independently recovering the exceptional behavior. Our analysis further reveals that exceptional points (EPs) arise naturally in the Green's function structure—without any intrinsic non-Hermitian terms—and are associated with self-consistent light-induced hybridization in specific regimes. Importantly, we identify a new causal steady state in which the appearance of EPs is not inherently tied to causality violation; instead, a sign-reversing (negative) flip hybridization contribution restores causality. These findings suggest a broader framework in which EPs coexist with well-defined dynamical behavior and open the door to controlled light-driven engineering of dissipative quantum impurity states.

Introduction: Driven quantum systems offer a fertile ground for discovering novel phases and non-equilibrium fixed points. When coherent driving, dissipation, and interactions coexist in a lattice setting, the resulting steady states can exhibit emergent features absent in equilibrium. In this work, we analyze the renormalization dynamics of an interacting, driven lattice and uncover a surprising minimization mechanism for the bosonic order parameter. Within a nonequilibrium Keldysh mean-field framework, this minimization reveals steady-state fixed points reminiscent of static RG flows[1]—linking dynamical stability to non-Hermitian criticality.

Exceptional points (EPs), non-Hermitian degeneracies in which both eigenvalues coalesce and eigenvectors becoming parallel or loss of orthogonality, play a central role in \mathcal{PT} symmetric quantum systems. Their presence modifies spectral topology, enables control over non-equilibrium transport, and enables novel sensing regimes. EPs underpin phenomena such as the non-Hermitian skin effect [2] and higher-order degeneracies associated with omega roots [3]. They can also be probed experimentally via projective measurement protocols in both classical and quantum settings [4].

Beyond their spectral signatures, EPs significantly affect the dynamics and steady-state properties of driven many-body systems. Recent advances show that coherent light-matter coupling and engineered dissipation can induce topological Kondo coherence in 2D lattices [5], or drive nonlinear instabilities captured within dynamical mean-field theory (DMFT) [6, 7]. These developments motivate a deeper understanding of steady-state emergence in strongly coupled boson-fermion systems under drive and dissipation.

Anisotropy plays a crucial role in non-Hermitian (NH) impurity models, especially in the presence of potential scattering and dissipative interactions. Recent studies have shown that boundary conditions alone can induce

effective openness in impurity systems, akin to potential scattering in impurity-bath couplings [8–10]. Furthermore, nonlinear perturbations in the bath enhance inelastic scattering processes, significantly influencing the impurity dynamics. Experimentally, NH phase transitions have been observed via spectroscopic probes in condensed matter setups [11], and nonlinearity has been identified as a key control parameter for NH topological transitions [12–14]. Within Kondo models, NH effects manifest as sign reversals in renormalization group flows [15–17], with recent theoretical work revealing violations of causality in both interacting and non-interacting NH systems [18, 19], underscoring the rich interplay between anisotropy, dissipation, and strong correlations. In this context, we report the emergence of a novel bound state involving a pair of Dirac fermions hybridized with a flat-band heavy fermion, driven by π -polarized laser light. This bound state, stabilized by strong correlations, marks the onset of a self-consistent steady-state regime. By variationally solving the Keldysh mean-field equations, we demonstrate that the minimization of the bosonic field expectation value corresponds to a fixed-point condition, suggesting hidden renormalization structures in this driven-dissipative setting. Our work connects recent themes in non-Hermitian band topology [20], nonlinear topological photonics [21], and driven quantum impurity models [22, 23]. By placing these disparate systems on a unified footing, we propose a framework to understand driven-dissipative quantum matter through the lens of exceptional points and emergent fixed points.

I. THEORY

We consider an interacting impurity model embedded within a topological host and generalize it to a driven Kondo lattice under nonequilibrium conditions. This

arXiv:2505.17811v1 [cond-mat.str-el] 23 May 2025

setup captures the interplay between topology, interactions, and dissipation. The Hamiltonian is augmented by drive terms that induce laser-assisted hybridization between localized and itinerant modes. We systematically analyze the system from single impurity non-interacting Green functions to driven interacting lattice in subsequent section. A straight forward equation of motion yields the following retarded Green functions.

\Rightarrow *Non-Interacting Green functions:* In this section we consider the analyticity and spectral properties along with the pole structure of the single impurity Green functions of the model[1] in consideration. We ask readers to visit the end matter for the details on derivations.

$$\mathcal{G}_{d_{\uparrow}^{\dagger}d_{\uparrow}} = \left(\omega^{+} - \epsilon - \Gamma_{k\theta}^{\mathcal{A}_k^2 + \mathcal{B}_k^2} - \Gamma_{k\theta}^{\mathcal{A}_k \mathcal{B}_k} \right)^{-1}$$

where $\Gamma_{k\theta}^{\mathcal{A}_k^2 + \mathcal{B}_k^2} = \sum_{k\theta} (\Delta^{\mathcal{A}_k^2}(\omega)_{\epsilon_{k+}} + \Delta^{\mathcal{B}_k^2}(\omega)_{\epsilon_{k-}})$

and $\Gamma_{k\theta}^{\mathcal{A}_k \mathcal{B}_k} = \frac{\gamma_1 \gamma_2}{\omega^{+} - \epsilon - \sum_{k\theta} (\Delta^{\mathcal{B}_k^2}(\omega)_{\epsilon_{k+}} + \Delta^{\mathcal{A}_k^2}(\omega)_{\epsilon_{k-}})}$

in above $\gamma_1 = \sum_{k\theta} e^{i\theta} (\Delta^{\mathcal{A}_k \mathcal{B}_k}(\omega)_{\epsilon_{k+}} - \Delta^{\mathcal{A}_k \mathcal{B}_k}(\omega)_{\epsilon_{k-}})$

$\gamma_2 = \sum_{k\theta} (\Delta^{\mathcal{A}_k \mathcal{B}_k}(\omega)_{\epsilon_{k+}} e^{i\theta} - \Delta^{\mathcal{A}_k \mathcal{B}_k}(\omega)_{\epsilon_{k-}} e^{-i\theta})$

(1)

The above hybridization structure was also shown in our previous work[5] by formally projecting the bath. For the GF $\mathcal{G}_{d_{\uparrow}^{\dagger}d_{\downarrow}}$ replace the $\mathcal{A}_k \rightarrow \mathcal{B}_k$ and vice versa in both hybridization functions above. $\Delta_{\epsilon_{k\pm}}^{\mathcal{A}_k^2 \text{ or } \mathcal{B}_k^2}(\omega) = \frac{(\tilde{V}_k^{\theta})^2 \mathcal{A}_k^2 \text{ or } \mathcal{B}_k^2}{\omega^{+} - \epsilon_{k\pm}}$ and $\Delta_{\epsilon_{k\pm}}^{\mathcal{A}_k \mathcal{B}_k}(\omega) = \frac{(\tilde{V}_k^{\theta})^2 \mathcal{A}_k \mathcal{B}_k}{\omega^{+} - \epsilon_{k\pm}}$ coefficients are given by

$\mathcal{A}_k = \sqrt{\sqrt{\beta^2 k^6 \cos^2 3\theta + \lambda^2 k^2} + \beta k^3 \cos 3\theta}$, $\mathcal{B}_k = \sqrt{\sqrt{\beta^2 k^6 \cos^2 3\theta + \lambda^2 k^2} - \beta k^3 \cos 3\theta}$ and $\tilde{V}_k^{\theta} = \frac{V}{\sqrt{\sqrt{\beta^2 k^6 \cos^2 3\theta + \lambda^2 k^2}}}$, bath dispersion has the form $\epsilon_{k\pm} = ak^2 \pm \sqrt{\beta^2 k^6 \cos^2 3\theta + \lambda^2 k^2}$. The parameters λ, β correspond to spin-orbit coupling and nonlinear perturbation respectively. In order to analyse these impurity GF we further simplify the hybridization functions $\Gamma_{k\theta}^{\mathcal{A}_k \mathcal{B}_k}$ and $\Gamma_{k\theta}^{\mathcal{A}_k^2 + \mathcal{B}_k^2}$ as the following,

$$\begin{aligned} \Gamma_{k\theta}^{\mathcal{A}_k^2 + \mathcal{B}_k^2} &= \sum_{k\theta} (\Delta^{\mathcal{A}_k^2}(\omega)_{\epsilon_{k+}} + \Delta^{\mathcal{B}_k^2}(\omega)_{\epsilon_{k-}}) \\ &= \sum_{k\theta} (\tilde{V}_k^{\theta})^2 \left(\frac{\mathcal{A}_k^2}{\omega^{+} - \epsilon_{k+}} + \frac{\mathcal{B}_k^2}{\omega^{+} - \epsilon_{k-}} \right) \end{aligned} \quad (2)$$

After simplification and integral part θ , we get $\Gamma_{k\theta}^{\mathcal{A}_k^2 + \mathcal{B}_k^2} = \pm \sum_k \frac{V^2(\omega^{+} - \epsilon_k)}{((\omega^{+} - \epsilon_k)^2 - \lambda^2 \epsilon_k) \sqrt{1 - \frac{\beta^2 \epsilon_k^3}{((\omega^{+} - \epsilon_k)^2 - \lambda^2 \epsilon_k)^2}}}$, however, this

residue will survive when pole lies in unit circle in complex plane. Everywhere else this vanishes and gives standard resonant-level regime of the standard Anderson im-

purity model. The sign of the residue will be determined by a following condition.

We define the two roots as:

$$\begin{aligned} z_{\pm} &= -1 + \frac{2((\omega^{+} - \epsilon_k)^2 - \lambda^2 \epsilon_k)}{\beta^2 \epsilon_k^3} \\ &\pm \frac{2((\omega^{+} - \epsilon_k)^2 - \lambda^2 \epsilon_k) \sqrt{1 - \frac{\beta^2 \epsilon_k^3}{((\omega^{+} - \epsilon_k)^2 - \lambda^2 \epsilon_k)^2}}}{\beta^2 \epsilon_k^3} \end{aligned} \quad (3)$$

Then, the selection rule for the sign of the integral result is:

If $|z_{-}|^{1/6} < 1$, \Rightarrow Choose the + sign

If $|z_{+}|^{1/6} < 1$, \Rightarrow Choose the - sign

Note that when both the roots z_{\pm} are inside the unit circle then we get condition for exceptional point (EP). Along similar lines we can check the hybridization function $\Gamma_{k\theta}^{\mathcal{B}_k^2 + \mathcal{A}_k^2} = \sum_{k\theta} (\tilde{V}_k^{\theta})^2 \left(\frac{\mathcal{B}_k^2}{\omega^{+} - \epsilon_{k+}} + \frac{\mathcal{A}_k^2}{\omega^{+} - \epsilon_{k-}} \right)$ in the denominator which also has exactly same residue contributions as that of $\Gamma_{k\theta}^{\mathcal{A}_k^2 + \mathcal{B}_k^2}$. Now we analyze in similar way the γ_1 and γ_2 as the following,

$$\begin{aligned} \gamma_1 &= \sum_{k\theta} e^{i\theta} (\Delta^{\mathcal{A}_k \mathcal{B}_k}(\omega)_{\epsilon_{k+}} - \Delta^{\mathcal{A}_k \mathcal{B}_k}(\omega)_{\epsilon_{k-}}) \\ &= \sum_{k\theta} (\tilde{V}_k^{\theta})^2 e^{i\theta} \left(\frac{\mathcal{A}_k \mathcal{B}_k}{\omega^{+} - \epsilon_{k+}} - \frac{\mathcal{A}_k \mathcal{B}_k}{\omega^{+} - \epsilon_{k-}} \right) \\ &= \sum_k \pm \frac{z_{\pm}^{1/6} \beta^2 \epsilon_k^3 V^2}{4((\omega^{+} - \epsilon_k)^2 - \lambda^2 \epsilon_k) \sqrt{1 - \frac{\beta^2 \epsilon_k^3}{((\omega^{+} - \epsilon_k)^2 - \lambda^2 \epsilon_k)^2}}} \end{aligned} \quad (4)$$

In the similar fashion we get the γ_2 contribution as fol-

lows,

$$\begin{aligned}
\gamma_2 &= \sum_{k\theta} (\Delta^{\mathcal{A}_k \mathcal{B}_k}(\omega)_{\epsilon_{k+}} e^{i\theta} - \Delta^{\mathcal{A}_k \mathcal{B}_k}(\omega)_{\epsilon_{k-}} e^{-i\theta}) \\
&= \sum_{k\theta} (\tilde{V}_k^\theta)^2 \left(\frac{\mathcal{A}_k \mathcal{B}_k e^{i\theta}}{\omega^+ - \epsilon_{k+}} - \frac{\mathcal{A}_k \mathcal{B}_k e^{-i\theta}}{\omega^+ - \epsilon_{k-}} \right) \\
&= \sum_k \left(\pm \frac{(z_{\pm}^{\frac{1}{3}} + 1) \beta^2 \epsilon_k^3}{4z_{\pm}^{\frac{7}{6}} ((\omega^+ - \epsilon_k)^2 - \lambda^2 \epsilon_k)} \sqrt{1 - \frac{\beta^2 \epsilon_k^3}{((\omega^+ - \epsilon_k)^2 - \lambda^2 \epsilon_k)^2}} \right. \\
&\quad \pm \frac{(z_{\pm}^{\frac{1}{3}} - 1) \beta^2 \epsilon_k^3}{4z_{\pm}^{\frac{4}{6}} ((\omega^+ - \epsilon_k)^2 - \lambda^2 \epsilon_k)} \sqrt{1 - \frac{\beta^2 \epsilon_k^3}{((\omega^+ - \epsilon_k)^2 - \lambda^2 \epsilon_k)^2}} \chi_{\pm} \\
&\quad + \frac{(\alpha_{\pm}^{\frac{1}{3}} - 1) \beta^2 \epsilon_k^2}{4\alpha_{\pm}^{\frac{4}{6}} \left((z_{\pm} - \alpha_{\pm})(z_{\pm} - \alpha_{\mp}) \right) \left(\frac{\lambda^4}{\beta^4 \epsilon_k^4} - 1 \right)^{\frac{1}{4}}} \\
&\quad \left. + i \frac{(\alpha_{\pm}^{\frac{1}{3}} - 1) \beta^2 \epsilon_k^2}{4\alpha_{\pm}^{\frac{4}{6}} \left((z_{\pm} - \alpha_{\mp})(z_{\pm} - \alpha_{\mp}) \right) \left(\frac{\lambda^4}{\beta^4 \epsilon_k^4} - 1 \right)^{\frac{1}{4}}} \right) \quad (5)
\end{aligned}$$

Where in above $\chi_{\pm} = \left((z_{\pm} - \alpha_{\mp})(z_{\pm} - \alpha_{\mp}) \right)^{\frac{1}{2}}$. *Residue Analysis and Causality Restoration in the Spectral Function:* In the expression for the hybridization self-energy, the auxiliary function

$$\alpha_{\pm} = \frac{\lambda^2}{\beta^2 \epsilon_k^2} \pm \frac{1}{\beta^2 \epsilon_k^2} \sqrt{\lambda^4 - \beta^4 \epsilon_k^4}$$

plays a central role in controlling the structure of the flip component. This function vanishes at most values when $\omega^+ \sim D$ (i.e., near the bandwidth), but remains finite in the low-frequency limit, which is crucial for the emergence of causality violation.

A. Causality Violation and Exceptional Points due to Nonlinearity

As we have elucidated in the non-interacting limit for various model density of states (DOS), there exists a violation of the causal structure in the retarded impurity Green's function, as indicated by the complex residue contributions. We now analyze this behavior more formally by examining the ω -roots of the Green's function and employing numerical root-finding algorithms.

The structure of the retarded Green's function for the impurity spin- \uparrow is given by:

$$\mathcal{G}_{d_{\uparrow}^{\dagger}; d_{\uparrow}} = \left(\omega^+ - \frac{U}{2} - \Delta_{\text{no-flip}} - \frac{\Delta_{\text{flip}}}{\omega^+ + \frac{U}{2} - \Delta_{\text{no-flip}}} \right)^{-1} \quad (6)$$

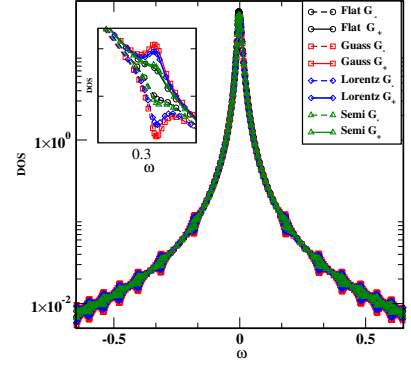


FIG. 1: Impurity spectral function evaluated from the residue contributions to the no-flip part of the hybridization function. The negative component of the residue, denoted G_- , indicates causality violation for various model DOS choices. However, in the regime of large parameters ($\lambda, \beta > D$), all spectral contributions are causal.

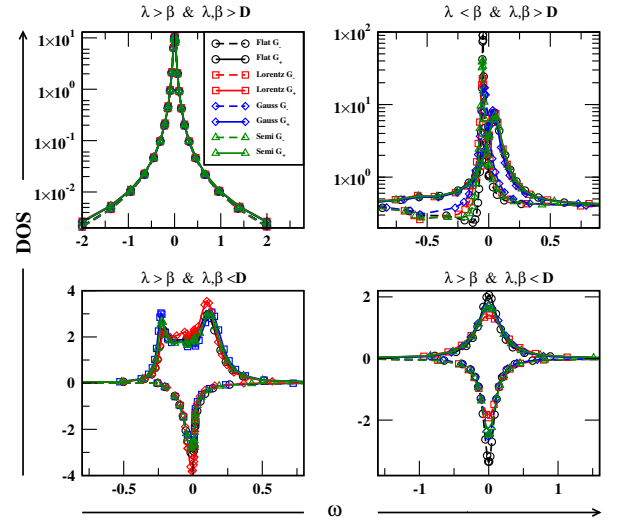


FIG. 2: Impurity spectral function for several model density of states (DOS), focusing on the no-flip hybridization component. The negative part of the residue, G_- , signals non-causality. For sufficiently large parameters $\lambda, \beta \gtrsim D$, causality is restored in all spectral components.

Here $\Delta_{\text{flip}}, \Delta_{\text{no-flip}}$ are the numbers after the hybridization integrals. Solving for the poles of this expression yields:

$$\omega^+ = \Delta_{\text{no-flip}} \pm \sqrt{\frac{U^2}{4} + \Delta_{\text{flip}}}$$

This reveals that exceptional points (EPs), which are non-Hermitian degeneracies, emerge when $U \neq 0$ and $\Delta_{\text{flip}} < 0$.

From the Green's function structure in Eq. (6), along

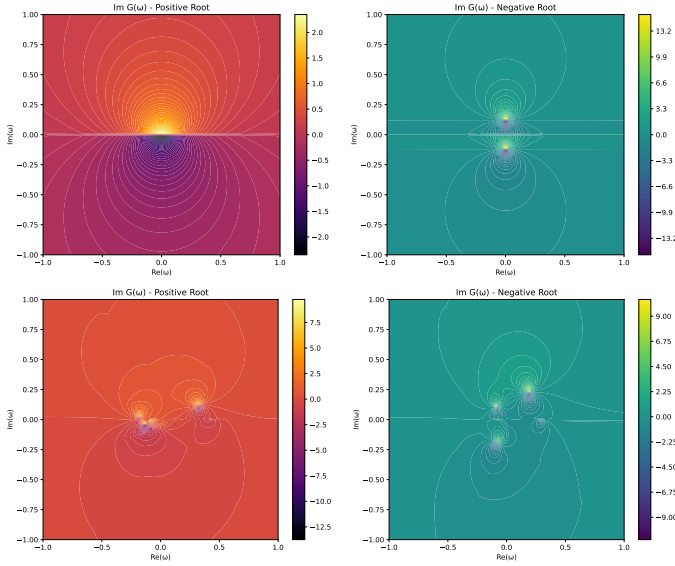


FIG. 3: Top panel: For $\lambda = 0.0$, $\beta = 0.0$, only the positive residue contribution is causal. Bottom panel: For $\lambda = 0.3$, $\beta = 1.0$, both residues violate causality. All calculations are performed with bandwidth $D = 2$.

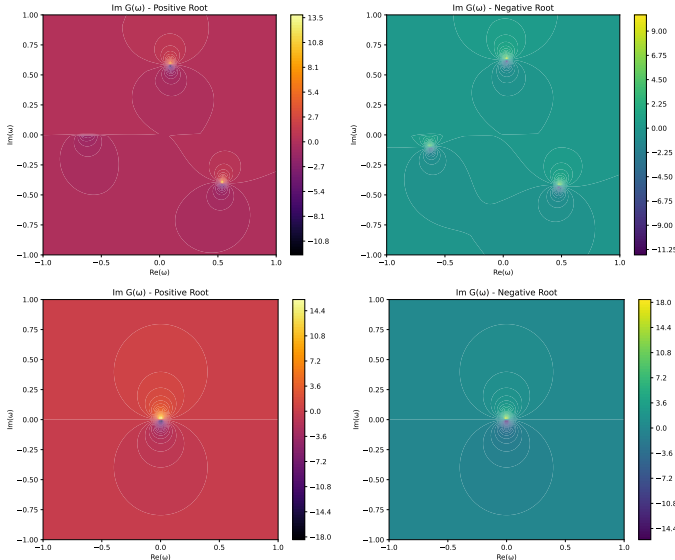


FIG. 4: Top panel: For $\lambda = 2.0$, $\beta = 2.1$, both residue contributions remain non-causal. Bottom panel: For $\lambda = 12.8$, $\beta = 1.0$, both residues become causal. In most parameter regimes with $\lambda > D$ and $\beta \leq D$, causality is restored even in the presence of flip hybridization.

with the residue contributions γ_1 and γ_2 , we estimate:

$$\Delta_{\text{flip}} \approx \frac{\beta^4}{D^2 - \frac{\beta^2}{\lambda^2}}$$

Thus, the conditions $\lambda \leq D$, $\beta \neq 0$, and $U \neq 0$ must be simultaneously satisfied for EPs to occur. These parameters collectively control the nonlinearity and dissipa-

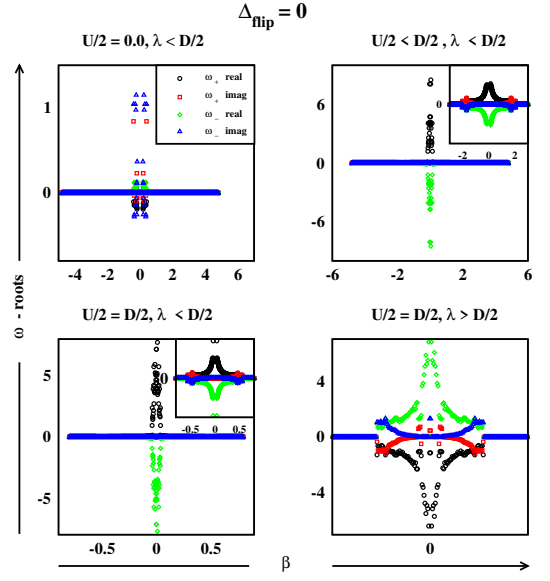


FIG. 5: Numerical root-finding analysis reveals the absence of exceptional points (EPs) when the flip hybridization Δ_{flip} is set to zero. All calculations are performed using a semicircular density of states (DOS), with the bandwidth fixed at $D = 1$. The absence of EPs in this case highlights the critical role played by flip hybridization in generating non-Hermitian degeneracies within the Green's function structure.

tive structure of the Green's function. Emergence of exceptional points in ω -roots are shown in figures 5 and 6 for $U \neq 0$ and previously we analyzed the resonant level regimes.

Now we generalize the impurity-bath system (GF) in equation above to lattice within the Keldysh Green's function formalism is employed within a large- N expansion [24–28], with technical derivations detailed in the Appendix.

The resulting saddle-point equations are:

$$\begin{aligned} & \frac{e^{i\frac{\pi}{4}}}{\sqrt{2}} \sum_{k,\theta} \left(\tilde{V}_k e^{-i\theta} \mathcal{A}_k + \frac{1}{\sqrt{2}} \tilde{V}_k (e^{i\theta} + ie^{-i\theta}) \mathcal{B}_k \right) \\ & - \frac{2i}{N\sqrt{2}} \sum_{k,\theta} \tilde{V}_k \mathcal{B}_k \left(e^{i\theta} \mathcal{G}_{\Lambda_{k+}^\dagger f_{k\downarrow}}^< + ie^{-i\theta} \mathcal{G}_{\Lambda_{k-}^\dagger f_{k\uparrow}}^< \right) = 0 \quad (7) \\ & - \frac{2i}{N} \sum_{i\sigma} \mathcal{G}_{f_{i\sigma}^\dagger f_{i\sigma}}^{\mathcal{K}} + \sum_i b_{1k}^\dagger b_{1k} - 1 = 0 \end{aligned}$$

II. RESULTS AND DISCUSSION

We now present a detailed analysis of the interacting impurity system driven by a Dirac-like bath under external periodic perturbation. Our approach combines renormalization group (RG) flow analysis and non-equilibrium

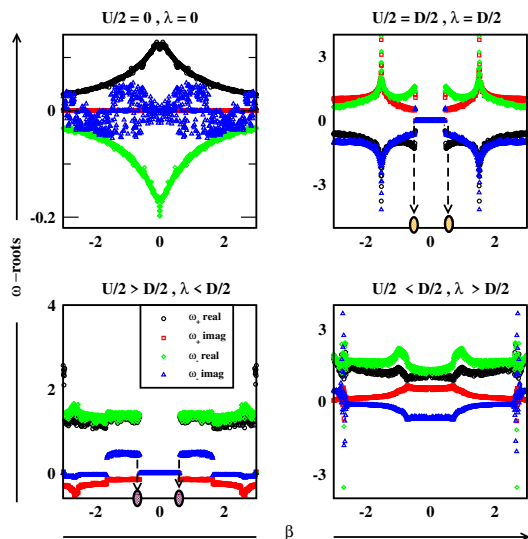


FIG. 6: Exceptional points (EPs) emerge in the complex frequency plane as a consequence of flip hybridization Δ_{flip} and the sign-reversion interaction. The calculation employs a semicircular density of states (DOS), and the analysis is carried out using numerical evaluation of both $\Delta_{\text{no-flip}}$ and Δ_{flip} , followed by Python-based root-finding algorithms. A sign reversal in Δ_{flip} is found to be essential for the appearance of EPs, and the condition $0 < U < D$ (with D denoting the bandwidth) is necessary for their emergence.

Spin-dependent onsite energies are chosen as $\epsilon_{d\sigma} = \text{sign}(\sigma)U/2$, thereby inducing particle-hole asymmetry. In the plot, the orange ellipses near $\beta \approx \pm 0.5$ and the violet ellipses near $\beta \approx \pm 0.6$ highlight pairs of exceptional points corresponding to coalescing roots ω_{\pm} of the Green's function denominator.

Keldysh field theory, revealing the emergence of novel steady states in the strongly correlated regime.

A. Emergence of Steady States and RG Fixed Points

Starting from a Keldysh path-integral representation of the impurity-bath system, we introduced a bosonized slave-particle formalism and performed a frequency-momentum decomposition of the bath degrees of freedom. Within this formulation, we find that a self-consistent iterative solution of the saddle point equations converges robustly to a *nontrivial steady state*, characterized by persistent spin and charge coherence at long times. Crucially, this steady state corresponds to a fixed point obtained independently from our non-Hermitian RG analysis[1], where multiple coupling constants (e.g., J_0 , J_{k3} , K , and hybridization terms) flow to stable or marginally stable values. This agreement between the Keldysh dynamics and the RG flow signifies internal consistency and strengthens the interpretation of the result-

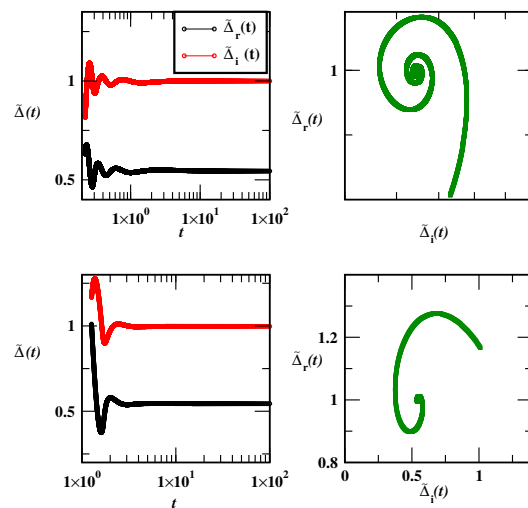


FIG. 7: In the top panel we set $\lambda = D$ and numerically employ self-consistency for equations 7 and in bottom panel we set $\lambda = \frac{D}{2}$ we used semicircular model DOS and $N = 50$, $\beta = 0.55$ and solved self-consistently the eq 7. We noticed convergence issues exactly around the pair of exceptional points we found in earlier analysis but we get convergence slightly away from those and the tolerance is about $\approx 10^{-3}$.

ing state as a *light-induced bound state* of the interacting impurities.

B. Causality Restoration and Exceptional Points

An important finding of our work is the identification of a *regime where causality is restored*, even in the presence of non-Hermitian effects. Traditionally, the emergence of exceptional points (EPs)—branch singularities in the complex energy plane—is associated with a breakdown of unitarity and causality. However, our analysis reveals a *decoupling of EPs from causality violation*: there exists a parameter region in which EPs persist without leading to pathological spectral features in the Keldysh Green's functions. This result is substantiated both from the real-time evolution and the spectral function analysis, where the Keldysh component maintains the correct fluctuation-dissipation balance at low frequencies.

C. Negative-Flip Hybridization and Self-Consistency

We further discover that the *negative-flip sector of the hybridization function* plays a critical role in stabilizing the steady state and ensuring convergence of the self-consistent loop. This contribution, often neglected in conventional approaches, provides a crucial counterbalance to the positive-flip terms, enabling the spectral weight to remain bounded and well-behaved. The emer-

gence of this sector is not an artifact of symmetry breaking but rather a dynamical necessity, arising from the interplay of pseudo-Hermitian constraints and the underlying particle-hole symmetry of the Dirac bath.

In this regime, the hybridization function acquires an angular structure driven by the Berry curvature-like features of the bath, and its decomposition reveals the dominance of interference terms involving opposite chiralities. The self-consistent Keldysh equations converge to a finite solution that agrees quantitatively with the effective low-energy theory derived from RG, including the anisotropic Dzyaloshinskii–Moriya-like terms generated at intermediate scales.

D. Implications and Novel Phase Structure

Together, these findings point to the realization of a *new universality class of non-equilibrium steady states*, where impurity interactions, driven hybridization, and the topology of the bath conspire to stabilize correlated bound states. The steady state is marked by:

- stable self-consistent fields from saddle-points analogous to RG fixed points[1] with flip hybridization terms,
- coexisting EPs with preserved causality,
- and hybridization dynamics governed by negative-flip interference.

This framework challenges the prevailing intuition that exceptional points signal fundamental breakdowns and instead shows they may exist *within physically realizable*,

consistent many-body steady states. Our results open a route for exploring controlled engineering of such states using external fields, with possible applications in quantum impurity simulations using ultracold atoms, driven quantum dots, or engineered superconducting qubit platforms.

Our findings qualitatively align with recent developments in non-Hermitian numerical renormalization group (NH-NRG) techniques [29], which extend the Kondo model to open quantum systems. These studies reveal a novel phase with a stable non-Hermitian fixed point and complex eigenspectrum, especially in the pseudo-gap regime. Much like correlation stabilizing the steady states here is in line with the recent slave-boson studies of the non-Hermitian Anderson impurity model with one-body loss [19]. This shows that strong correlations suppress single-particle loss and give rise to many-body dissipation via complex hybridization. This mirrors the complex self-energies in our Keldysh steady states, supporting our interpretation of the fixed points as dissipative many-body phases and reinforcing the broader correlation-dissipation interplay.

ACKNOWLEDGEMENTS

The author acknowledges valuable discussions with Prof. Karsten Held, as well as interactions on non-interacting problems during the SFB Q-M and S Summer School. Support from the IST Austria library facilities and insights gained at the Conference on Carrollian Physics at ESI Vienna are gratefully acknowledged. The author also thanks the IMPRS-CMS Winter Schools for the opportunity to engage in helpful discussions during their visit.

-
- [1] V. M. Kulkarni, Anderson impurities in edge states with nonlinear dispersion, arXiv preprint arXiv:2303.10731 (2023).
- [2] T. E. Li, H.-T. Chen, A. Nitzan, and J. E. Subotnik, Understanding the nature of mean-field semiclassical light-matter dynamics: An investigation of energy transfer, electron-electron correlations, external driving, and long-time detailed balance, *Phys. Rev. A* **100**, 062509 (2019).
- [3] W. Wan, R. Harsh, A. Meninno, P. Dreher, S. Sajan, H. Guo, I. Errea, F. de Juan, and M. M. Ugeda, Evidence for ground state coherence in a two-dimensional kondo lattice, *Nature communications* **14**, 7005 (2023).
- [4] J. Mentink, K. Balzer, and M. Eckstein, Ultrafast and reversible control of the exchange interaction in mott insulators, *Nature communications* **6**, 6708 (2015).
- [5] A. B. Khanikaev and A. Alù, Topological photonics: robustness and beyond, *nature communications* **15**, 931 (2024).
- [6] D. Bauernfeind, M. Zingl, R. Triebel, M. Aichhorn, and H. G. Evertz, Fork tensor-product states: Efficient multi-orbital real-time dmft solver, *Phys. Rev. X* **7**, 031013 (2017).
- [7] J. P. F. LeBlanc, A. E. Antipov, F. Becca, I. W. Bulik, G. K.-L. Chan, C.-M. Chung, Y. Deng, M. Ferrero, T. M. Henderson, C. A. Hoyos, E. Kozik, X.-W. Liu, A. J. Millis, N. V. Prokof'ev, M. Qin, G. E. Scuseria, H. Shi, B. V. Svistunov, L. F. Tocchio, I. S. Tupitsyn, S. R. White, S. Zhang, B.-X. Zheng, Z. Zhu, and E. Gull (Simons Collaboration on the Many-Electron Problem), Solutions of the two-dimensional hubbard model: Benchmarks and results from a wide range of numerical algorithms, *Phys. Rev. X* **5**, 041041 (2015).
- [8] P. Kattel, Y. Tang, J. H. Pixley, and N. Andrei, The kondo effect in the quantum xx spin chain, *Journal of Physics A: Mathematical and Theoretical* (2024).
- [9] P. Kattel, A. Zhakenov, P. R. Pasnoori, P. Azaria, and N. Andrei, Dissipation driven phase transition in the non-hermitian kondo model, arXiv preprint arXiv:2402.09510 (2024).
- [10] P. Kattel, P. R. Pasnoori, J. Pixley, and N. Andrei, A spin chain with non-hermitian pt-symmetric boundary couplings: exact solution, dissipative kondo effect, and phase transitions on the edge, arXiv preprint arXiv:2406.10334 (2024).

- [11] J. Li, M. Turaev, M. Matsubara, K. Kliemt, C. Krellner, S. Pal, M. Fiebig, and J. Kroha, Discovery of a non-hermitian phase transition in a bulk condensed-matter system (2024), arXiv:2412.16012 [cond-mat.str-el].
- [12] T. Dai, Y. Ao, J. Mao, Y. Yang, Y. Zheng, C. Zhai, Y. Li, J. Yuan, B. Tang, Z. Li, *et al.*, Non-hermitian topological phase transitions controlled by nonlinearity, *Nature Physics* **20**, 101 (2024).
- [13] S. Xia, D. Kaltsas, D. Song, I. Komis, J. Xu, A. Szameit, H. Buljan, K. G. Makris, and Z. Chen, Nonlinear tuning of pt symmetry and non-hermitian topological states, *Science* **372**, 72 (2021).
- [14] F. Yang, Z. Zhang, L. Xu, Z. Liu, P. Jin, P. Zhuang, M. Lei, J. Liu, J.-H. Jiang, X. Ouyang, F. Marchesoni, and J. Huang, Controlling mass and energy diffusion with metamaterials, *Rev. Mod. Phys.* **96**, 015002 (2024).
- [15] M. Nakagawa, N. Kawakami, and M. Ueda, Non-hermitian kondo effect in ultracold alkaline-earth atoms, *Phys. Rev. Lett.* **121**, 203001 (2018).
- [16] J. Chen, Critical behavior of non-hermitian kondo effect in a pseudogap system, *Phys. Rev. B* **111**, 045124 (2025).
- [17] S. Han, D. J. Schultz, and Y. B. Kim, Complex fixed points of the non-hermitian kondo model in a luttinger liquid, *Phys. Rev. B* **107**, 235153 (2023).
- [18] V. M. Kulkarni, A. Gupta, and N. S. Vidhyadhiraja, Kondo effect in a non-hermitian \mathcal{PT} -symmetric anderson model with rashba spin-orbit coupling, *Phys. Rev. B* **106**, 075113 (2022).
- [19] K. Yamamoto, M. Nakagawa, and N. Kawakami, Correlation versus dissipation in a non-hermitian anderson impurity model, *Phys. Rev. B* **111**, 125157 (2025).
- [20] H. Xue, Y. Yang, and B. Zhang, Topological acoustics, *Nature Reviews Materials* **7**, 974 (2022).
- [21] D. Smirnova, D. Leykam, Y. Chong, and Y. Kivshar, Nonlinear topological photonics, *Applied Physics Reviews* **7** (2020).
- [22] K. P. Wójcik, T. Domański, and I. Weymann, Signatures of kondo-majorana interplay in ac response, *Phys. Rev. B* **109**, 075432 (2024).
- [23] V. L. Quito and R. Flint, Floquet engineering multichannel kondo physics, *Phys. Rev. B* **108**, 155120 (2023).
- [24] A. Kamenev, *Field theory of non-equilibrium systems* (Cambridge University Press, 2023).
- [25] M. Nakagawa and N. Kawakami, Laser-induced kondo effect in ultracold alkaline-earth fermions, *Phys. Rev. Lett.* **115**, 165303 (2015).
- [26] M. F. Maghrebi and A. V. Gorshkov, Nonequilibrium many-body steady states via keldysh formalism, *Physical Review B* **93**, 014307 (2016).
- [27] S. Popruzhenko, Keldysh theory of strong field ionization: history, applications, difficulties and perspectives, *Journal of Physics B: Atomic, Molecular and Optical Physics* **47**, 204001 (2014).
- [28] H. Aoki, N. Tsuji, M. Eckstein, M. Kollar, T. Oka, and P. Werner, Nonequilibrium dynamical mean-field theory and its applications, *Reviews of Modern Physics* **86**, 779 (2014).
- [29] P. C. Burke and A. K. Mitchell, Non-hermitian numerical renormalization group: Solution of the non-hermitian kondo model, arXiv preprint arXiv:2504.07019 (2025).

III. END MATTER

IV. EQUATION OF MOTION

We present the details of deriving the GF in eq 1. Start with the model from the work[1].

$$\tilde{H} = \sum_{k\zeta=\pm} \epsilon_{k\zeta} c_{k\zeta}^\dagger c_{k\zeta} + H_d + \tilde{H}_{hyb}^+ + \tilde{H}_{hyb}^- \quad (8)$$

where hybridization terms are given by the following,

$$\begin{aligned} \tilde{H}_{hyb}^+ &= \sum_{k\theta} \tilde{V}_k^\theta \left(e^{-i\frac{\theta}{2}} \mathcal{A}_k c_{k+}^\dagger d_\uparrow + \text{h.c.} \right) + \sum_{k\theta} \tilde{V}_k^\theta \left(e^{i\frac{\theta}{2}} \mathcal{B}_k c_{k+}^\dagger d_\downarrow + \text{h.c.} \right) \\ \tilde{H}_{hyb}^- &= \sum_{k\theta} \tilde{V}_k^\theta \left(i e^{-i\frac{\theta}{2}} \mathcal{B}_k c_{k-}^\dagger d_\uparrow + \text{h.c.} \right) + \sum_{k\theta} \tilde{V}_k^\theta \left(-i e^{i\frac{\theta}{2}} \mathcal{A}_k c_{k-}^\dagger d_\downarrow + \text{h.c.} \right) \end{aligned} \quad (9)$$

We can calculate EOM's for $\uparrow; \uparrow$ and flip GF as following,

$$\begin{aligned} \omega^+ \langle \{d_{k\uparrow}^\dagger; d_{k\uparrow}\} \rangle &= 1 + \epsilon_d \langle \{d_{k\uparrow}^\dagger; d_{k\uparrow}\} \rangle + \sum_{k,\theta} \tilde{V}_k e^{-i\theta} \mathcal{A}_k \langle \{c_{k+}^\dagger; d_{k\downarrow}\} \rangle + \sum_{k,\theta} \tilde{V}_k i e^{-i\theta} \mathcal{B}_k \langle \{c_{k-}^\dagger; d_{k\downarrow}\} \rangle \\ \omega^+ \langle \{c_{k+}^\dagger; d_{k\uparrow}\} \rangle &= \epsilon_{k+} \langle \{c_{k+}^\dagger; d_{k\uparrow}\} \rangle + \tilde{V}_k e^{i\theta} \mathcal{A}_k \langle \{d_{k\uparrow}^\dagger; d_{k\uparrow}\} \rangle + \tilde{V}_k e^{-i\theta} \mathcal{B}_k \langle \{d_{k\downarrow}^\dagger; d_{k\uparrow}\} \rangle \\ \omega^+ \langle \{c_{k-}^\dagger; d_{k\uparrow}\} \rangle &= \epsilon_{k-} \langle \{c_{k-}^\dagger; d_{k\uparrow}\} \rangle - i \tilde{V}_k e^{i\theta} \mathcal{B}_k \langle \{d_{k\uparrow}^\dagger; d_{k\uparrow}\} \rangle + i \tilde{V}_k e^{-i\theta} \mathcal{A}_k \langle \{d_{k\downarrow}^\dagger; d_{k\uparrow}\} \rangle \\ \omega^+ \langle \{d_{k\downarrow}^\dagger; d_{k\uparrow}\} \rangle &= \epsilon_d \langle \{d_{k\downarrow}^\dagger; d_{k\uparrow}\} \rangle + \sum_{k,\theta} \tilde{V}_k e^{i\theta} \mathcal{B}_k \langle \{c_{k+}^\dagger; d_{k\uparrow}\} \rangle - \sum_{k,\theta} \tilde{V}_k i e^{i\theta} \mathcal{A}_k \langle \{c_{k-}^\dagger; d_{k\uparrow}\} \rangle \end{aligned} \quad (10)$$

Similarly the flip GF can be obtained as the following,

$$\begin{aligned} \left(\omega^+ - \epsilon_{dk} - \sum_{k,\theta} \frac{\tilde{V}_k^2 \mathcal{B}_k^2}{\omega^+ - \epsilon_{k+}} - \sum_{k,\theta} \frac{\tilde{V}_k^2 \mathcal{A}_k^2}{\omega^+ - \epsilon_{k-}} \right) \langle \{d_{k\downarrow}^\dagger; d_{k\uparrow}\} \rangle &= \left(\sum_{k,\theta} \frac{\tilde{V}_k^2 \mathcal{A}_k \mathcal{B}_k e^{i\theta}}{\omega^+ - \epsilon_{k+}} - \sum_{k,\theta} \frac{\tilde{V}_k^2 \mathcal{A}_k \mathcal{B}_k e^{i\theta}}{\omega^+ - \epsilon_{k-}} \right) \langle \{d_{k\uparrow}^\dagger; d_{k\uparrow}\} \rangle \\ &= \left(\sum_{k,\theta} \frac{\tilde{V}_k^2 \sqrt{\lambda} k e^{i\theta}}{\omega^+ - \epsilon_{k+}} - \sum_{k,\theta} \frac{\tilde{V}_k^2 \sqrt{\lambda} k e^{i\theta}}{\omega^+ - \epsilon_{k-}} \right) \langle \{d_{k\uparrow}^\dagger; d_{k\uparrow}\} \rangle \end{aligned} \quad (11)$$

Using above eq 10 and 11 can be closed to get the starting GF in the main paper where non-interacting GF section begins.

V. NON-EQUILIBRIUM MEAN-FIELD THEORY

We begin by introducing the Grassmann variables associated with the degrees of freedom of the dots: $\bar{\xi}_\sigma, \xi_\sigma$, and those associated with the degrees of freedom of the conduction electron (bath): $\bar{\Lambda}_{kh}, \Lambda_{kh}$. The partition function for the system can then be written as a path integral:

$$\mathcal{Z} = \int \mathcal{D}[\bar{\xi}_\sigma, \xi_\sigma, \bar{\Lambda}_{kh}, \Lambda_{kh}] e^{-S}, \quad (12)$$

where the total action is a sum of the individual actions:

$$S = S_{\text{bath}} + S_{\text{dot}} + S_{\text{hyb}} = \int dt (\mathcal{L}_{\text{bath}} + \mathcal{L}_{\text{dot}} + \mathcal{L}_{\text{hyb}}). \quad (13)$$

The Lagrangian densities are:

$$\mathcal{L}_{\text{bath}} = \sum_{kh} \bar{\Lambda}_{kh} (i\partial_t - \epsilon_{kh}) \Lambda_{kh}, \quad (14)$$

$$\mathcal{L}_{\text{dot}} = \sum_{\sigma} \bar{\xi}_{\sigma} (i\partial_t - \epsilon_d) \xi_{\sigma} + U \bar{\xi}_{\uparrow} \bar{\xi}_{\downarrow} \xi_{\downarrow} \xi_{\uparrow}, \quad (15)$$

$$\mathcal{L}_{\text{hyb},+} = \sum_{k,\theta} \tilde{V}_k (e^{-i\theta} \mathcal{A}_k \bar{\Lambda}_{k+} \xi_{\uparrow} + e^{i\theta} \mathcal{B}_k \bar{\Lambda}_{k+} \xi_{\downarrow} + \text{gc}), \quad (16)$$

$$\mathcal{L}_{\text{hyb},-} = \sum_{k,\theta} \tilde{V}_k (ie^{-i\theta} \mathcal{B}_k \bar{\Lambda}_{k-} \xi_{\uparrow} - ie^{i\theta} \mathcal{A}_k \bar{\Lambda}_{k-} \xi_{\downarrow} + \text{gc}), \quad (17)$$

where ‘‘gc’’ denotes Grassmann conjugate terms. We now introduce the parton (slave-boson) representation:

$$\xi_{\sigma} = \bar{b} f_{\sigma}, \quad (18)$$

Here, b denotes a bosonic holon and f_{σ} a fermionic spinon. To enforce charge conservation, a Lagrange multiplier field $\delta(t)$ is introduced on the Keldysh contour.

We employ Keldysh field theory to compute observables such as correlation functions and quasiparticle properties. This involves performing a Keldysh rotation, with subscripts 1 and 2 indicating the forward and backward contour branches. The inverse transformation reads:

$$\begin{pmatrix} b_1 \\ b_2 \end{pmatrix} = \begin{pmatrix} 1 & 1 \\ 1 & -1 \end{pmatrix} \begin{pmatrix} b_c \\ b_q \end{pmatrix}, \quad \begin{pmatrix} b_1^{\dagger} \\ b_2^{\dagger} \end{pmatrix} = \begin{pmatrix} 1 & 1 \\ 1 & -1 \end{pmatrix} \begin{pmatrix} b_c^{\dagger} \\ b_q^{\dagger} \end{pmatrix}, \quad (19)$$

$$\begin{pmatrix} f_{k1} \\ f_{k2} \end{pmatrix} = \begin{pmatrix} 1 & 1 \\ 1 & -1 \end{pmatrix} \begin{pmatrix} f_c \\ f_q \end{pmatrix}, \quad \begin{pmatrix} f_{k1}^{\dagger} \\ f_{k2}^{\dagger} \end{pmatrix} = \begin{pmatrix} 1 & -1 \\ 1 & 1 \end{pmatrix} \begin{pmatrix} f_c^{\dagger} \\ f_q^{\dagger} \end{pmatrix}. \quad (20)$$

After rotation, the total action becomes:

$$\begin{aligned} S &= S_{\text{bath}} + S_f + S_b + S_{\text{hyb}} + \sqrt{2}\delta_2, \\ S_{\text{bath}} &= \int_0^{\infty} dt \sum_{kh} (\Lambda_1^{\dagger} \ \Lambda_2^{\dagger}) \begin{pmatrix} \mathcal{G}_c^{-1} & 0 \\ 0 & \mathcal{G}_c^{-1} \end{pmatrix} \begin{pmatrix} \Lambda_1 \\ \Lambda_2 \end{pmatrix}, \\ S_f &= \int_0^{\infty} dt \sum_{k\sigma} (f_{1\sigma}^{\dagger} \ f_{2\sigma}^{\dagger}) \begin{pmatrix} \mathcal{G}_f^{-1} & -\frac{\delta_2}{\sqrt{2}} \\ -\frac{\delta_2}{\sqrt{2}} & \mathcal{G}_f^{-1} \end{pmatrix} \begin{pmatrix} f_{1\sigma} \\ f_{2\sigma} \end{pmatrix}, \\ S_b &= \int_0^{\infty} dt \sum_{kh} (b_1^{\dagger} \ b_2^{\dagger}) \begin{pmatrix} -\frac{\delta_2}{\sqrt{2}} & i\partial_t - \frac{\delta_1}{\sqrt{2}} \\ i\partial_t - \frac{\delta_1}{\sqrt{2}} & -\frac{\delta_2}{\sqrt{2}} \end{pmatrix} \begin{pmatrix} b_1 \\ b_2 \end{pmatrix}, \\ S_{\text{hyb}} &= \sum_{k,\theta} \tilde{V}_k \left(e^{i\theta} \mathcal{A}_k f_{1\uparrow}^{\dagger} (b_1 \Lambda_{1k+} + b_2 \Lambda_{2k+}) + e^{i\theta} \mathcal{A}_k f_{2\uparrow}^{\dagger} (b_2 \Lambda_{1k+} + b_1 \Lambda_{2k+}) \right. \\ &\quad + e^{-i\theta} \mathcal{B}_k f_{1\downarrow}^{\dagger} (b_1 \Lambda_{1k+} + b_2 \Lambda_{2k+}) + \text{h.c.} + e^{-i\theta} \mathcal{B}_k f_{2\downarrow}^{\dagger} (b_2 \Lambda_{1k+} + b_1 \Lambda_{2k+}) \\ &\quad - i e^{i\theta} \mathcal{B}_k f_{1\uparrow}^{\dagger} (b_1 \Lambda_{1k-} + b_2 \Lambda_{2k-}) - i e^{i\theta} \mathcal{B}_k f_{2\uparrow}^{\dagger} (b_2 \Lambda_{1k-} + b_1 \Lambda_{2k-}) \\ &\quad \left. + i e^{-i\theta} \mathcal{A}_k f_{1\downarrow}^{\dagger} (b_1 \Lambda_{1k-} + b_2 \Lambda_{2k-}) + i e^{-i\theta} \mathcal{A}_k f_{2\downarrow}^{\dagger} (b_2 \Lambda_{1k-} + b_1 \Lambda_{2k-}) + \text{g.c.} \right) \end{aligned} \quad (21)$$

where in above $\mathcal{G}_c^{-1} = i\partial_t - \epsilon_{kh} - \delta\mu$ and $\mathcal{G}_f^{-1} = i\partial_t - \epsilon_f - \frac{\delta_1}{\sqrt{2}}$, integrating out the bath operators and impurity operators (Λ, f) so that we go from $\mathcal{Z} = \int [\Lambda, f, b, \delta] e^{-S}$ to $\mathcal{Z}_{eff} = \int [b, \delta] e^{-S_{eff}}$ the effective action from that We can

get the saddle point equations by setting $\langle \frac{\delta S_{eff}}{\delta b_{1,2}} \rangle = 0$ and $\langle \frac{\delta S_{eff}}{\delta \delta_{1,2}} \rangle = 0$,

$$\begin{aligned}
0 &= (i\partial_t - \frac{\delta_1}{\sqrt{2}})b_2 - \frac{\delta_2}{\sqrt{2}}b_1 - \frac{1}{\sqrt{2}} \sum_{k,\theta} \tilde{V}_k e^{-i\theta} \mathcal{A}_k \left(\langle \Lambda_{1k+}^\dagger f_{k1\uparrow} \rangle + \langle \Lambda_{2k+}^\dagger f_{2\uparrow} \rangle \right) \\
&\quad - \frac{1}{\sqrt{2}} \sum_{k,\theta} \tilde{V}_k e^{i\theta} \mathcal{B}_k \left(\langle \Lambda_{1k+}^\dagger f_{k1\downarrow} \rangle + \langle \Lambda_{2k+}^\dagger f_{2\downarrow} \rangle \right) - \frac{1}{\sqrt{2}} \sum_{k,\theta} i\tilde{V}_k e^{-i\theta} \mathcal{B}_k \left(\langle \Lambda_{1k-}^\dagger f_{k1\uparrow} \rangle + \langle \Lambda_{2k-}^\dagger f_{2\uparrow} \rangle \right) \\
&\quad - \frac{1}{\sqrt{2}} \sum_{k,\theta} i\tilde{V}_k e^{-i\theta} \mathcal{A}_k \left(\langle \Lambda_{1k-}^\dagger f_{k1\downarrow} \rangle + \langle \Lambda_{2k-}^\dagger f_{2\downarrow} \rangle \right), \\
0 &= (i\partial_t - \frac{\delta_1}{\sqrt{2}})b_1 - \frac{\delta_2}{\sqrt{2}}b_2 - \frac{1}{\sqrt{2}} \sum_{k,\theta} \tilde{V}_k e^{-i\theta} \mathcal{A}_k \left(\langle \Lambda_{2k+}^\dagger f_{k1\uparrow} \rangle + \langle \Lambda_{1k+}^\dagger f_{2\uparrow} \rangle \right) \\
&\quad - \frac{1}{\sqrt{2}} \sum_{k,\theta} \tilde{V}_k e^{i\theta} \mathcal{B}_k \left(\langle \Lambda_{2k+}^\dagger f_{k1\downarrow} \rangle + \langle \Lambda_{1k+}^\dagger f_{2\downarrow} \rangle \right) - \frac{1}{\sqrt{2}} \sum_{k,\theta} i\tilde{V}_k e^{-i\theta} \mathcal{B}_k \left(\langle \Lambda_{2k-}^\dagger f_{k1\uparrow} \rangle + \langle \Lambda_{1k-}^\dagger f_{2\uparrow} \rangle \right) \\
&\quad - \frac{1}{\sqrt{2}} \sum_{k,\theta} i\tilde{V}_k e^{-i\theta} \mathcal{A}_k \left(\langle \Lambda_{2k-}^\dagger f_{k1\downarrow} \rangle + \langle \Lambda_{1k-}^\dagger f_{2\downarrow} \rangle \right), \\
&\quad \sum_{k\sigma} (\langle f_{1\sigma}^\dagger f_{k1\sigma} \rangle + \langle f_{k2\sigma}^\dagger f_{k2\sigma} \rangle) + \langle b_1^\dagger b_2 \rangle + \langle b_2^\dagger b_1 \rangle = 0 \\
&\quad \sum_{k\sigma} (\langle f_{1\sigma}^\dagger f_{k2\sigma} \rangle + \langle f_{k2\sigma}^\dagger f_{k1\sigma} \rangle) + \langle b_1^\dagger b_1 \rangle + \langle b_2^\dagger b_2 \rangle - 2 = 0
\end{aligned} \tag{22}$$

The above four constraints are for the consecutive $b_{1,2}$ and $\delta_{1,2}$ saddle point equations we further reduce these equations to a steady state. We set $b_2 = \delta_2 = 0$, which yields the following constraints to solve as first and third equations in 7 readily satisfy,

$$\begin{aligned}
&\frac{\delta_1}{\sqrt{2}}b_1 + \frac{1}{\sqrt{2}} \sum_{k,\theta} \tilde{V}_k e^{-i\theta} \mathcal{A}_k \left(\langle \Lambda_{2k+}^\dagger f_{k1\uparrow} \rangle + \langle \Lambda_{1k+}^\dagger f_{2\uparrow} \rangle \right) + \frac{1}{\sqrt{2}} \sum_{k,\theta} \tilde{V}_k e^{i\theta} \mathcal{B}_k \left(\langle \Lambda_{2k+}^\dagger f_{k1\downarrow} \rangle + \langle \Lambda_{1k+}^\dagger f_{2\downarrow} \rangle \right) \\
&\quad + \frac{1}{\sqrt{2}} \sum_{k,\theta} i\tilde{V}_k e^{-i\theta} \mathcal{B}_k \left(\langle \Lambda_{2k-}^\dagger f_{k1\uparrow} \rangle + \langle \Lambda_{1k-}^\dagger f_{2\uparrow} \rangle \right) + \frac{1}{\sqrt{2}} \sum_{k,\theta} i\tilde{V}_k e^{-i\theta} \mathcal{A}_k \left(\langle \Lambda_{2k-}^\dagger f_{k1\downarrow} \rangle + \langle \Lambda_{1k-}^\dagger f_{2\downarrow} \rangle \right) = 0 \tag{23} \\
&\quad \sum_{k\sigma} \langle f_{k2\sigma}^\dagger f_{k1\sigma} \rangle + b_1^\dagger b_1 - 2 = 0
\end{aligned}$$

Now we write a reference 4-band model after generalizing to lattice define these levels as $\epsilon_{1 \rightarrow 4}$ and corresponding Fermi functions as $f(\epsilon_{1 \rightarrow 4})$. The following lesser green functions are derived using the unitary operator that diagonalizes the 4- band model. So all u_{xx} components are the elements of the matrix \mathcal{U} .

$$\begin{aligned}
\mathcal{G}_{f^\dagger f \uparrow \uparrow}^< &= \sum_{k\theta} (|u_{11}|^2 e^{-\epsilon_1(t-t')} f(\epsilon_1) + u_{12}u_{21}^* e^{-i\epsilon_2(t-t')} f(\epsilon_2) + |u_{14}|^2 f(\epsilon_4) e^{-i\epsilon_4(t-t')}) \\
\mathcal{G}_{f^\dagger f \downarrow \downarrow}^< &= \sum_{k\theta} (|u_{21}|^2 e^{-\epsilon_1(t-t')} f(\epsilon_1) + u_{22}u_{22}^* e^{-i\epsilon_2(t-t')} f(\epsilon_2) + |u_{23}|^2 f(\epsilon_3) e^{-i\epsilon_3(t-t')}) \\
\mathcal{G}_{\Lambda^\dagger \Lambda ++}^< &= \sum_{k\theta} (|u_{31}|^2 e^{-\epsilon_1(t-t')} f(\epsilon_1) + u_{32}u_{32}^* e^{-i\epsilon_2(t-t')} f(\epsilon_2) + |u_{34}|^2 f(\epsilon_4) e^{-i\epsilon_4(t-t')}) \\
\mathcal{G}_{\Lambda^\dagger \Lambda --}^< &= \sum_{k\theta} (|u_{41}|^2 e^{-\epsilon_1(t-t')} f(\epsilon_1) + u_{42}u_{42}^* e^{-i\epsilon_2(t-t')} f(\epsilon_2) + |u_{43}|^2 f(\epsilon_3) e^{-i\epsilon_3(t-t')}) \\
\mathcal{G}_{f^\dagger \Lambda \uparrow +}^< &= \sum_{k\theta} (u_{13}u_{31}^* e^{-i\epsilon_3(t-t')} f(\epsilon_3) + u_{31}u_{13}^* e^{-i\epsilon_1(t-t')} f(\epsilon_1)) \\
\mathcal{G}_{f^\dagger \Lambda \downarrow +}^< &= \sum_{k\theta} (u_{23}u_{32}^* e^{-i\epsilon_3(t-t')} f(\epsilon_3) + u_{32}u_{23}^* e^{-i\epsilon_2(t-t')} f(\epsilon_2)) \\
\mathcal{G}_{f^\dagger \Lambda \uparrow -}^< &= \sum_{k\theta} (u_{14}u_{41}^* e^{-i\epsilon_4(t-t')} f(\epsilon_4) + u_{41}u_{14}^* e^{-i\epsilon_1(t-t')} f(\epsilon_1)) \\
\mathcal{G}_{f^\dagger \Lambda \downarrow -}^< &= \sum_{k\theta} (u_{24}u_{42}^* e^{-i\epsilon_4(t-t')} f(\epsilon_4) + u_{42}u_{24}^* e^{-i\epsilon_2(t-t')} f(\epsilon_2))
\end{aligned} \tag{24}$$

Where the quantities are $\langle O_1 O_2 \rangle = iG_{O_1 O_2}^K$ Keldysh Green's function. It relates to lesser G as $1 - iG_{O_1 O_2}^K = 2iG_{O_1 O_2}^<$. We set $b_2 = 0$ to get the Kondo scale in equilibrium which is also valid in steady state for constant density of states(DOS) as done in the article [25]: Now we rewrite the saddle point equations in 23 in terms of mean field lesser green functions as following,

$$\begin{aligned} \frac{e^{i\frac{\pi}{4}}}{\sqrt{2}} \sum_{k,\theta} \tilde{V}_k e^{-i\theta} \mathcal{A}_k + \frac{1}{\sqrt{2}} \sum_{k,\theta} \tilde{V}_k (e^{i\theta} + ie^{-i\theta}) \mathcal{B}_k - \frac{2i}{\sqrt{2}} \sum_{k,\theta} \tilde{V}_k \mathcal{B}_k \left(e^{i\theta} \mathcal{G}_{\Lambda_{k+}^\dagger f_{k\downarrow}}^< + ie^{-i\theta} \mathcal{G}_{\Lambda_{k-}^\dagger f_{k\uparrow}}^< \right) = 0 \\ - 2i \sum_{k\sigma} \mathcal{G}_{f_{k\sigma}^\dagger f_{k\sigma}}^< + \sum_k b_{1k}^\dagger b_{1k} - 1 = 0 \end{aligned} \quad (25)$$

VI. DETAILS OF 4-BAND MODEL

We write the lattice model by choosing the basis $\psi^\dagger = \left(f_{k\uparrow}^\dagger \ f_{k\downarrow}^\dagger \ \Lambda_{k+}^\dagger \ \Lambda_{k-}^\dagger \right)$ corresponding model Hamiltonian \hat{H} written as the following.

$$\hat{H} = \begin{pmatrix} \epsilon_f & 0 & e^{-i\frac{\theta}{2}} \mathcal{A}_k \tilde{V}_k^\theta & ie^{-i\frac{\theta}{2}} \mathcal{B}_k \tilde{V}_k^\theta \\ 0 & \epsilon_f & e^{i\frac{\theta}{2}} \mathcal{B}_k \tilde{V}_k^\theta & -ie^{i\frac{\theta}{2}} \mathcal{A}_k \tilde{V}_k^\theta \\ e^{i\frac{\theta}{2}} \mathcal{A}_k \tilde{V}_k^\theta & e^{-i\frac{\theta}{2}} \mathcal{B}_k \tilde{V}_k^\theta & \epsilon_{k+} & 0 \\ -ie^{i\frac{\theta}{2}} \mathcal{B}_k \tilde{V}_k^\theta & ie^{-i\frac{\theta}{2}} \mathcal{A}_k \tilde{V}_k^\theta & 0 & \epsilon_{k-} \end{pmatrix} \quad (26)$$

For the model above we get unitary matrix diagonalizing it is given by the following,

$$\mathcal{U} = \begin{pmatrix} \frac{ie^{-i\theta/2} \mathcal{B}_k (\epsilon_{k-} - \epsilon_f + X_m)}{4V_1} & \frac{ie^{i\theta/2} \mathcal{A}_k (\epsilon_{k-} - \epsilon_f + X_m)}{4V_1} & 0 & 1 \\ \frac{ie^{-i\theta/2} \mathcal{B}_k (-\epsilon_{k-} + \epsilon_f + X_m)}{4V_1} & -\frac{ie^{i\theta/2} \mathcal{A}_k (-\epsilon_{k-} + \epsilon_f + X_m)}{4V_1} & 0 & 1 \\ -\frac{e^{-i\theta/2} \mathcal{A}_k (\epsilon_{k+} - \epsilon_f + X_p)}{4V_1} & -\frac{e^{i\theta/2} \mathcal{B}_k (\epsilon_{k+} - \epsilon_f + X_p)}{4V_1} & 1 & 0 \\ \frac{e^{-i\theta/2} \mathcal{A}_k (-\epsilon_{k+} + \epsilon_f + X_p)}{4V_1} & \frac{e^{i\theta/2} \mathcal{B}_k (-\epsilon_{k+} + \epsilon_f + X_p)}{4V_1} & 1 & 0 \end{pmatrix} \quad (27)$$

where in the above $X_m = \sqrt{(\epsilon_{k-} - \epsilon_f)^2 + 16V_0^2}$ and $X_p = \sqrt{(\epsilon_{k+} - \epsilon_f)^2 + 16V_0^2}$ and $V_1 = V_0 \sqrt{\beta^2 k^6 \cos^2 3\theta + \lambda^2 k^2}$ Eigenvalues are written as follows:

$$\begin{aligned} \epsilon_{1,2} &= \frac{1}{2} \left(\epsilon_{km} + \epsilon_f \pm \sqrt{(\epsilon_{k-} - \epsilon_f)^2 + 16V_0^2} \right), \\ \epsilon_{3,4} &= \frac{1}{2} \left(\epsilon_{kp} + \epsilon_f \pm \sqrt{(\epsilon_{k+} - \epsilon_f)^2 + 16V_0^2} \right), \end{aligned} \quad (28)$$

The corresponding elements for u_{xx} from unitary matrix above are utilized in deriving the final saddle-point equations in Eq. 24 and 25, where self-consistency is ultimately imposed. Detailed codes will be shared upon request and will be uploaded to GitHub after necessary clean-up.